Doublon-holon binding, Mott transition, and fractionalized antiferromagnet in the Hubbard model

Sen Zhou,[1,2,*] Yupeng Wang,[3] and Ziqiang Wang[2]

[1]*State Key Laboratory of Theoretical Physics, Institute of Theoretical Physics, Chinese Academy of Sciences, Beijing 100190, China*

[2]*Department of Physics, Boston College, Chestnut Hill, Massachusetts 02467, USA*

[3]*The Institute of Physics, Chinese Academy of Sciences, Beijing 100190, China*

(Received 20 September 2013; revised manuscript received 18 March 2014; published 15 May 2014)

We argue that the binding between doubly occupied (doublon) and empty (holon) sites governs incoherent excitations and plays a key role in the Mott transition in strongly correlated Mott-Hubbard systems. We construct a new saddle-point solution with doublon-holon binding in the Kotliar-Ruckenstein slave-boson functional integral formulation of the Hubbard model. On a half-filled honeycomb lattice and square lattice, the ground state is found to exhibit a continuous transition from a paramagnetic semimetal/metal to an antiferromagnetic-ordered Slater insulator with coherent quasiparticles at U_{c1}, followed by a Mott transition into an electron-fractionalized AF* phase without coherent excitations at U_{c2}. Such a phase structure appears to be generic for bipartite lattices without frustration. We show that doublon-holon binding unites the three important ideas of strong correlation: coherent quasiparticles, incoherent Hubbard bands, and deconfined Mott insulator.

DOI: 10.1103/PhysRevB.89.195119 PACS number(s): 71.27.+a, 71.10.Fd, 71.30.+h

I. INTRODUCTION

The fundamental theoretical challenge of the strong correlation problem is the description of both low-energy coherent quasiparticles (QPs) and higher energy incoherent excitations and spectral weight transfer from coherent to incoherent excitations with increasing correlation strength. Two very important ideas, the emergence of two broad incoherent features known as Hubbard bands and the existence of renormalized QPs with a Luttinger Fermi surface, were advanced by Hubbard [1] and Brinkman and Rice [2], respectively. Unfortunately, the Hubbard equation-of-motion scheme that produces an incoherent spectrum fails to produce QPs correctly and violates Luttinger's theorem [3], whereas the approaches based on the BR-Gutzwiller wave functions [4] capture a Luttinger Fermi surface of QPs but encounter serious difficulties in constructing variational excited states to account for the incoherent excitations. Faced with this enigma, numerical approaches such as exact diagonalization (ED), quantum Monte Carlo (QMC), and dynamical mean-field theory (DMFT) [5] have played a key role in recent studies of the strong correlation problem.

In this paper, we develop new analytical insights and construct a unified theory for both the coherent and the incoherent excitations as well as the magnetic and the Mott transition. Our focus is the half-filled single-band Hubbard model on bipartite lattices without frustration. As specific examples, we study the square lattice and the honeycomb lattice, especially in view of the recent debate over the possible emergence of a gapped spin-liquid (SL) phase on the honeycomb lattice [6–15]. With only on-site interactions, the Hilbert space of the Hubbard model is a product of the local Hilbert space on a single site that consists of empty (holon), doubly occupied (doublon), and singly occupied states. The BR-Gutzwiller approach amounts to a metallic state where the holon, denoted as a boson e, and the doublon, as d, condense fully with macroscopic phase coherence, as can be obtained by the Gutzwiller approximation [16] or the slave-boson mean-field theory [17]. The metal-insulator transition is thus forced to follow a route where the *densities* of doublons and holons vanish together with the condensates, $n_d = n_e = \langle d\rangle = \langle e\rangle = 0$, such that there is *exactly* one electron per site. As a result, single-particle motion, coherent or incoherent, is completely prohibited. This so-called Brinkman-Rice (BR) transition is different from the Mott transition induced by the complete transfer of the coherent QP weight into the incoherent background, i.e., depletion of the condensate with maintenance of the finite doublon/holon (D/H) *density* in the Mott insulator.

We show that the crucial physics uniting the disparate ideas of Hubbard and BR is the binding between doublon and holon: $\langle d_i e_j\rangle \neq 0$. In the Mott insulator at large U, although the D/H condensate vanishes ($\langle d\rangle = \langle e\rangle = d_0 = 0$), together with the disappearance of the coherent QP, the D/H density remains nonzero ($n_d = n_e \neq 0$). The motion of the QP is thus possible by breaking the D-H pairs, giving rise to higher energy incoherent excitations. With decreasing U, the D/H density increases and the D-H binding energy decreases. At a critical U_c, the D-H excitation gap closes and a D/H single-particle condensate develops, marking the onset of the Mott transition. On the metallic side of the Mott transition, D-H binding continues to play an important role since an added electron can propagate either as a coherent QP via the D/H condensate or incoherently via the unbinding of the D-H pairs.

The idea that D-H binding plays an important role in Mott-Hubbard systems was introduced by Kaplan, Horch, and Fulde [18] and studied in the context of improved variational Gutzwiller wave functions [19,20]. The difficulty in constructing appropriate variational wave functions for excitations has prevented further advances along these lines. More recently, field theory approaches involving the binding of charge $2e$ doublons with fermionic QPs [21] as well as combination of bosons with fermions to form cofermions [22] have been put forth within the context of doped Mott insulators.

In this work, we show that the physical picture presented above can be realized in the slave-boson functional integral formulation of the Hubbard model introduced by Kotliar and Ruckenstein (KR) [17] by constructing new saddle-point

*zhousen@itp.ac.cn

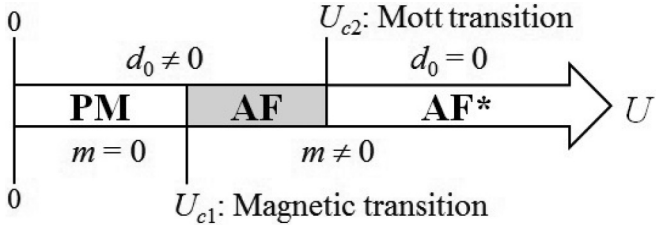

FIG. 1. Schematic phase diagram obtained for the half-filled single-band Hubbard model with D-H binding on a honeycomb lattice and a square lattice. The AF order m is developed after the magnetic transition U_{c1}, and the single-boson condensate of the doublon d_0 disappears at the Mott transition U_{c2}.

solutions that include D-H binding. This approach also offers a treatment of the magnetism at half-filling that compares well to QMC simulations [23] and has the added advantage of allowing the study of excitations and finite-temperature properties [24]. As concrete examples, we studied D-H binding in the half-filled Hubbard model on a honeycomb and a square lattice at zero temperature and obtained the phase diagram shown schematically in Fig. 1. On the honeycomb lattice, a continuous transition from a semimetal (SM) to an antiferromagnetic (AF)-ordered insulator takes place at a critical Coulomb repulsion $U_{c1} \simeq 3.4t$, suggesting that the gapped SL phase proposed by Meng *et al*. [6] may correspond to an AF-ordered phase in the thermodynamic limit. Sorella *et al.* [12] recently extended the QMC and the finite-size scaling analysis to much larger system sizes and discovered that the signature of the gapped SL disappears and is replaced by that of a continuous SM-to-AF order transition at $U \simeq 3.8t$, in qualitative agreement with our results. Remarkably, we found a second quantum phase transition at a critical $U_{c2} \simeq 5.7t$ beyond which the D/H single-particle condensate vanishes ($d_0 = 0$) amid a finite density of doublons bound to holons. For $U > U_{c2}$, a new AF phase without coherent QP excitations, termed AF* in Fig. 1, emerges where the electrons are fractionalized and the elementary excitations do not carry the quantum numbers of an electron. We obtained a similar phase diagram for the square lattice; the transition to the Slater AF state happens for infinitesimal U (i.e., $U_{c1} = 0$) due to the perfect nesting of the Fermi surface on the square lattice, while the transition to the AF* phase takes place at $U_{c2} \simeq 6.8t$.

The rest of the paper is organized as follows. Section II describes the slave-boson path integral formulation of the Hubbard model, the KR saddle-point solution on the honeycomb and the square lattice, and the BR metal-insulator transition. In Sec. III, we introduce the slave-boson intersite correlations into the functional integral and construct the new saddle-point solution that includes the effects of D-H binding. The Mott transition and the spectral weight transfer between coherent and incoherent excitations are studied to obtain the phase diagrams of the Hubbard model on the two half-filled bipartite lattices. We describe the transitions among the paramagnetic (PM) metal/SM, Slator AF insulator, and AF* phases, elucidate the properties of the electron-fractionalized AF* phase, and develop further insights into the nature of the incoherent excitations in Mott-Hubbard systems. Section IV contains the summary and conclusions.

II. HUBBARD MODEL AND SLAVE-BOSON FUNCTIONAL INTEGRAL REPRESENTATION

We start with the Hubbard model with nearest-neighbor hopping t and on-site Coulomb repulsion U,

$$\hat{H} = -t \sum_{\langle i,j\rangle,\sigma} (c^\dagger_{i\sigma} c_{j\sigma} + \text{H.c.}) + U \sum_i \hat{n}_{i\uparrow}\hat{n}_{i\downarrow}, \tag{1}$$

where $c^\dagger_{i\sigma}$ creates an electron with spin σ on site i, and $\hat{n}_{i\sigma} = c^\dagger_{i\sigma} c_{i\sigma}$ is the density operator. In the KR formulation [17], the electron operator is written as

$$c_{i\sigma} = \hat{z}_{i\sigma} f_{i\sigma}, \quad \hat{z}_{i\sigma} = \hat{L}_{i\sigma}(e^\dagger_i p_{i\sigma} + p^\dagger_{i\bar{\sigma}} d_i)\hat{R}_{i\sigma}, \tag{2}$$

where the boson operators describe the holon (e_i), doublon (d_i), and singly occupied ($p_{i\sigma}$) sites, and $f_{i\sigma}$ is a fermion operator. The operators $\hat{L}_\sigma$ and $\hat{R}_\sigma$ are diagonal with unit eigenvalues in the (empty; $\bar{\sigma}$) and the (σ; doubly occupied) subspaces, respectively [29],

$$\hat{L}_{i\sigma} = (1 - d^\dagger_i d_i - p^\dagger_{i\sigma} p_{i\sigma})^\alpha, \quad \hat{R}_{i\sigma} = (1 - e^\dagger_i e_i - p^\dagger_{i\bar{\sigma}} p_{i\bar{\sigma}})^\beta,$$

where α and β can take any value. The Hubbard-model Hamiltonian is thus given by

$$\hat{H}_{\text{KR}} = -t \sum_{\langle i,j\rangle,\sigma} (\hat{z}^\dagger_{i\sigma}\hat{z}_{j\sigma} f^\dagger_{i\sigma} f_{j\sigma} + \text{H.c.}) + U \sum_i d^\dagger_i d_i. \tag{3}$$

The partition function is a coherent-state path integral over the quantum fields [30].

$$Z = \int \mathcal{D}[f,f^\dagger]\mathcal{D}[e,e^\dagger]\mathcal{D}[p,p^\dagger]\mathcal{D}[d,d^\dagger]\mathcal{D}[\lambda,\lambda_\sigma] e^{-\int_0^\beta \mathcal{L} d\tau}, \tag{4}$$

where the Lagrangian is given by

$$\mathcal{L} = \sum_i (e^\dagger_i \partial_\tau e_i + d^\dagger_i \partial_\tau d_i) + \sum_{i,\sigma} (p^\dagger_{i\sigma} \partial_\tau p_{i\sigma} + f^\dagger_{i\sigma} \partial_\tau f_{i\sigma}) + \hat{H}_{\text{KR}} + i \sum_i \lambda_i \hat{Q}_i + i \sum_{i,\sigma} \lambda_{i\sigma} \hat{Q}_{i\sigma} - \mu \sum_{i\sigma} f^\dagger_{i\sigma} f_{i\sigma}, \tag{5}$$

where μ is the chemical potential and λ_i and $\lambda_{i\sigma}$ are the Lagrange multipliers introduced to enforce the local constraints for the completeness of the Hilbert space,

$$\hat{Q}_i = e^\dagger_i e_i + \sum_\sigma p^\dagger_{i\sigma} p_{i\sigma} + d^\dagger_i d_i - 1 = 0, \tag{6}$$

and the equivalence between the fermion and the boson representations of the spin-dependent density

$$\hat{Q}_{i\sigma} = f^\dagger_{i\sigma} f_{i\sigma} - p^\dagger_{i\sigma} p_{i\sigma} - d^\dagger_i d_i = 0. \tag{7}$$

The KR saddle point corresponds to condensing all the boson fields uniformly, with their values determined by minimizing the action [17]. KR found that for $\alpha = \beta = -1/2$, the saddle-point solution recovers the Gutzwiller approximation [17].

The KR saddle-point solutions on a half-filled honeycomb lattice [31] are summarized in Fig. 2. Restricting ourselves to the PM phase, the doublon density d_0^2 decreases linearly from $1/4$ at $U = 0$ and vanishes at the BR metal-insulator transition $U_{\text{BR}} \simeq 12.6t$. When magnetism is allowed, an SM–to–AF

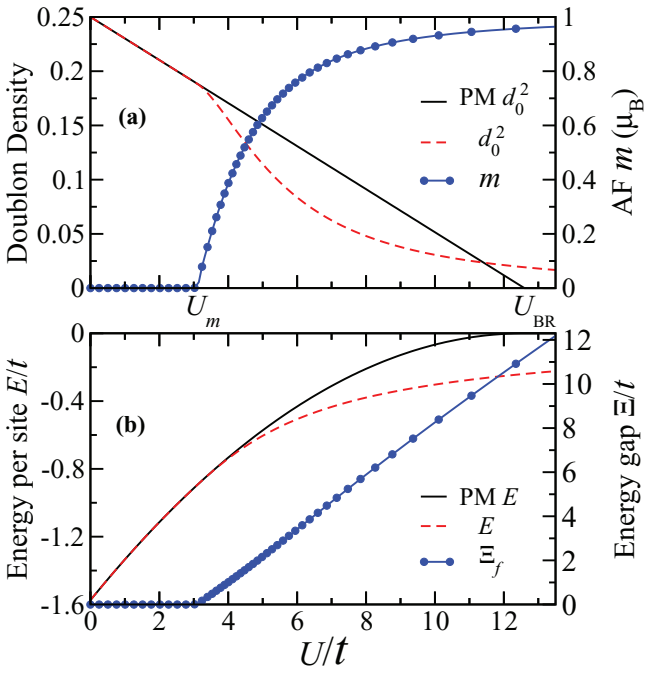

FIG. 2. (Color online) KR saddle-point solutions of the Hubbard model on a half-filled honeycomb lattice. The Hubbard U dependence of (a) the doublon condensate density d_0^2 and staggered magnetization m and (b) the energy per site E and single-particle energy gap in the fermion sector Ξ_f. Corresponding results in the restricted PM phase are also shown.

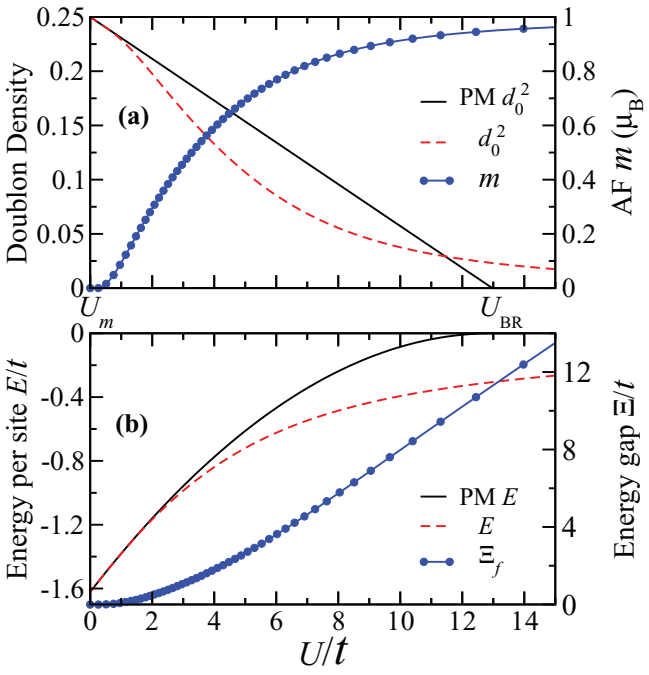

FIG. 3. (Color online) KR saddle-point solutions of the Hubbard model on a half-filled square lattice. Labels and notations follow those in Fig. 2.

insulator transition arises at $U_m \simeq 3.1t$. The D/H condensate remains nonzero for all finite U and the AF phase is a Slater insulator with coherent QP excitations. The results on a half-filled square lattice are shown in Fig. 3. The BR metal-insulator takes place at $U_{\rm BR} \simeq 13t$. When magnetism is allowed, the PM metal is unstable with respect to the Slator AF insulator for any nonzero U owing to the perfect nesting of the Fermi surface; the AF-ordered moment develops exponentially at $U_m = 0$.

III. BOSON INTERSITE CORRELATIONS AND NEW SADDLE-POINT SOLUTIONS WITH DOUBLON-HOLON BINDING

The KR saddle-point solution, i.e., the Gutzwiller approximation, ignores all intersite correlations and captures only the coherent QP single-particle excitations. Indeed, it has been shown [32] that in the limit of infinite dimensions (infinite d), the latter becomes an exact solution of the variational Gutzwiller wave-function approach. Our strategy for going beyond the Gutzwiller approximation described by the KR saddle point is to build in explicitly the intersite correlations and boson dynamics in the functional integral and construct a new saddle-point solution that includes D-H binding.

A. Path integral including boson intersite correlations

Introducing the operators for the D-H pairing, $\hat{\Delta}_{ij} = d_i e_j$, and the D/H hopping $\hat{\chi}^d_{ij} = d_i^\dagger d_j$, $\hat{\chi}^e_{ij} = e_i^\dagger e_j$ on the nearest-neighbor bonds, as well as the density operators $\hat{n}^d_i = d_i^\dagger d_i$, $\hat{n}^e_i = e_i^\dagger e_i$ on each site, we can rewrite the bosonic part in the hopping term in Eq. (3) as

$$\hat{z}^\dagger_{i\sigma}\hat{z}_{j\sigma} = \hat{Y}^{-1/2}_{ij,\sigma}\big[(\hat{\chi}^e_{ij})^\dagger p^\dagger_{i\sigma}p_{j\sigma} + \hat{\chi}^d_{ij}p_{i\bar{\sigma}}p^\dagger_{j\bar{\sigma}} + \hat{\Delta}_{ji}p^\dagger_{i\sigma}p^\dagger_{j\bar{\sigma}} + \hat{\Delta}^\dagger_{ij}p_{i\bar{\sigma}}p_{j\sigma}\big]\hat{Y}^{-1/2}_{ji,\sigma}, \quad (8)$$

where

$$\hat{Y}_{ij,\sigma} = \hat{R}^{-2}_{i\sigma}\hat{L}^{-2}_{j\sigma} = \big[(1-p^\dagger_{i\bar{\sigma}}p_{i\bar{\sigma}})(1-p^\dagger_{j\sigma}p_{j\sigma}) - \hat{n}^e_i(1-p^\dagger_{j\sigma}p_{j\sigma}) - \hat{n}^d_j(1-p^\dagger_{i\bar{\sigma}}p_{i\bar{\sigma}}) + |\hat{\Delta}_{ji}|^2\big]. \quad (9)$$

Note that, due to the normal ordering of the square roots, the expression for $\hat{Y}_{ij,\sigma}$ involves explicitly the D-H pairing but not the H/D hopping operators. The obvious challenge is how to build these correlations into the calculation of the partition function. Since they enter through the rather formidable factor $\hat{z}^\dagger_{i\sigma}\hat{z}_{j\sigma}$, the usual procedure of introducing the corresponding correlation fields (Δ_{ij}, $\chi^e_{i,j}$, χ^d_{ij}, n^d_i, n^e_i) via Hubbard-Stratonovich transformations in the path integral does not work here. We found that the difficulty can be overcome by introducing in the functional integral additional Lagrange multipliers in the corresponding channel, $\Delta^{\rm v}_{ij}$, $\chi^{d,{\rm v}}_{ij}$, $\chi^{e,{\rm v}}_{ij}$, $\epsilon^{d,{\rm v}}_i$, and $\epsilon^{e,{\rm v}}_i$, such that the partition function becomes

$$Z = \int \mathcal{D}[f,f^\dagger]\mathcal{D}[e,e^\dagger]\mathcal{D}[p,p^\dagger]\mathcal{D}[d,d^\dagger]\mathcal{D}[\lambda,\lambda_\sigma] \times \mathcal{D}[\Delta,\chi^d,\chi^e,n^d,n^e]\mathcal{D}[\Delta^{\rm v},\chi^{d,{\rm v}},\chi^{e,{\rm v}},\epsilon^{d,{\rm v}}\epsilon^{e,{\rm v}}]e^{-\int_0^\beta d\tau\mathcal{L}}, \quad (10)$$

with the Lagrangian

$$\mathcal{L} = \sum_i (e_i^\dagger \partial_\tau e_i + d_i^\dagger \partial_\tau d_i) + \sum_{i,\sigma} (p_{i\sigma}^\dagger \partial_\tau p_{i\sigma} + f_{i\sigma}^\dagger \partial_\tau f_{i\sigma}) + \hat{H}_{\rm DH} + i \sum_i \lambda_i \hat{Q}_i + i \sum_{i,\sigma} \lambda_{i\sigma} \hat{Q}_{i\sigma} - \mu \sum_{i\sigma} f_{i\sigma}^\dagger f_{j\sigma}, \tag{11}$$

where $\hat{H}_{\rm DH}$ is the effective D-H binding Hamiltonian

$$\begin{aligned}\hat{H}_{\rm DH} = &-t \sum_{\langle i,j\rangle,\sigma} (z_{i\sigma} z_{j\sigma} f_{i\sigma}^\dagger f_{j\sigma} + \text{H.c.}) + U \sum_i d_i^\dagger d_i \\ &- i \sum_{\langle i,j\rangle} \big[\chi_{ij}^{d,\text{v}} \big(d_i^\dagger d_j - \chi_{ij}^d\big) + \chi_{ij}^{e,\text{v}} \big(e_i^\dagger e_j - \chi_{ij}^e\big) \\ &+ \Delta_{ij}^\text{v} (d_i e_j - \Delta_{ij}) + \Delta_{ji}^\text{v} (e_i d_j - \Delta_{ji}) + \text{H.c.}\big] \\ &+ i \sum_i \big[\epsilon_i^{d,\text{v}} \big(d_i^\dagger d_i - n_i^d\big) + \epsilon_i^{e,\text{v}} \big(e_i^\dagger e_i - n_i^e\big)\big]. \end{aligned} \tag{12}$$

The factor $z_{i\sigma} z_{j\sigma}$ in Eq. (12) has the same form given in Eqs. (8) and (9) but with the bosonic operators replaced by their corresponding correlation fields $(\Delta_{ij}, \chi_{i,j}^e, \chi_{ij}^d, n_i^d, n_i^e)$. A few remarks are in order. (i) Equations (10)–(12) provide an exact representation of the Hubbard model; carrying out formally the last two functional integrals in Eq. (10) recovers the KR formulation given in Eqs. (3)–(5). (ii) The intersite correlations of the $p_{i\sigma}$ bosons can be included in a similar manner. For simplicity, we treat the latter as condensed fields in this paper since their densities (i.e., the density of single occupations) remain high at half-filling. (iii) From the perspective of finding a saddle-point solution of the action, the effective Hamiltonian $H_{\rm DH}$ in Eq. (12) can be understood intuitively as a variational Hamiltonian describing the effects of intersite correlations of the doublons and holons, including that of D-H binding, where Δ_{ij}^v, $\chi_{ij}^{d,\text{v}}$, $\chi_{ij}^{e,\text{v}}$, $\epsilon_i^{d,\text{v}}$, and $\epsilon_i^{e,\text{v}}$ are nothing but the variational parameters to be self-consistently determined.

B. Saddle-point solutions with D-H binding

We next discuss the D-H binding saddle-point solutions of the path integral in Eqs. (10)–(12) which correspond to configurations of the quantum fields that minimize the action. We consider here the translation-invariant PM and the two-sublattice AF saddle-point solutions on the half-filled bipartite (honeycomb and square) lattices with $2N$ sites. The bond variables are taken to be real and isotropic, and symmetry requires $\Delta_{\langle ij\rangle} = \Delta_d$, $\chi_{\langle ij\rangle}^d = \chi_{\langle ij\rangle}^e = \chi_d$, $n_i^d = n_i^e = n_d$, and correspondingly, $i\Delta_{\langle ij\rangle}^\text{v} = \Delta_d^\text{v}$, $i\chi_{\langle ij\rangle}^{d,\text{v}} = i\chi_{\langle ij\rangle}^{e,\text{v}} = \chi_d^\text{v}$, $i\epsilon_i^{d,\text{v}} = i\epsilon_i^{e,\text{v}} = \epsilon_d^\text{v}$. Moreover $i\lambda_i = \lambda$, $i\lambda_{A\sigma} = i\lambda_{B\bar{\sigma}} = \lambda_\sigma$, and $p_{A0\sigma} = p_{B0\bar{\sigma}} = p_{0\sigma}$, where A and B denote the two sublattices on the bipartite lattice. Consequently, on the nearest-neighbor bonds $\langle i,j\rangle$, the factor

$$t z_{i\sigma} z_{j\sigma} = tg\big[2p_{0\uparrow} p_{0\downarrow} \chi_d + \big(p_{0\uparrow}^2 + p_{0\downarrow}^2\big)\Delta_d\big] \equiv \chi_f^\text{v}, \tag{13}$$

where $g = \prod_\sigma Y_\sigma^{-1/2}$, with

$$Y_\sigma = 1 - 2n_d - 2p_{0\sigma}^2 + 2p_{0\sigma}^2 n_d + p_{0\sigma}^4 + \Delta_d^2. \tag{14}$$

As shown later, this expression ensures that the new saddle-point solution recovers the noninteracting limit at $U = 0$. Substituting these quantities into Eq. (12), we obtain the saddle-point Hamiltonian,

$$\begin{aligned}\hat{H}_{\rm DH}^{\rm sp} = &\hat{H}_f + \hat{H}_d + 4N\zeta\big(\chi_d^\text{v} \chi_d + \Delta_d^\text{v} \Delta_d\big) \\ &- 2N\big(\epsilon_d^\text{v} + 2\lambda\big) - 4N\epsilon_d^\text{v} n_d + 2N \sum_\sigma (\lambda - \lambda_\sigma) p_{0\sigma}^2, \end{aligned} \tag{15}$$

where the coordination number $\zeta = 3$ on the honeycomb lattice and $\zeta = 4$ on the square lattice. The Hamiltonian $\hat{H}_f$ and $\hat{H}_d$ determine the energy spectra in the fermion and boson sectors, respectively.

1. Fermion spectrum

The fermion spectrum is given by, in terms of the wave vector $\mathbf{k}$ defined on the reciprocal lattice,

$$\hat{H}_f = \sum_{\mathbf{k},\sigma} \begin{bmatrix} f_{A\mathbf{k}\sigma} \\ f_{B\mathbf{k}\sigma} \end{bmatrix}^\dagger \begin{bmatrix} \lambda_\sigma - \mu & -\chi_f^\text{v} \eta_\mathbf{k} \\ -\chi_f^\text{v} \eta_\mathbf{k}^* & \lambda_{\bar{\sigma}} - \mu \end{bmatrix} \begin{bmatrix} f_{A\mathbf{k}\sigma} \\ f_{B\mathbf{k}\sigma} \end{bmatrix}, \tag{16}$$

where $\eta_\mathbf{k}$ is the dispersion due to the nearest-neighbor hopping t, which takes the form of

$$\eta_\mathbf{k} = \exp(ik_y) + 2\cos(\sqrt{3}k_x/2)\exp(-ik_y/2)$$

on the honeycomb lattice and

$$\eta_\mathbf{k} = 2(\cos k_x + \cos k_y)$$

on the square lattice. The sum over $\mathbf{k}$ runs over the first Brillouin zone, corresponding to a unit cell with two sites. The particle-hole symmetry at half-filling requires $\mu = U/2$ and $\lambda_\sigma = \mu - \sigma\varepsilon$, where $\varepsilon = (\lambda_\uparrow - \lambda_\downarrow)/2$ becomes nonzero when AF order develops. The fermion dispersion is thus obtained by diagonalizing Eq. (16):

$$E_\pm^f(\mathbf{k}) = \pm\sqrt{\varepsilon^2 + \big|\chi_\mathbf{f}^\text{v} \eta_\mathbf{k}\big|^2}. \tag{17}$$

A gap of $\Xi_f = 2|\varepsilon|$ would open in the fermion spectrum in the presence of AF order.

On the square lattice, the sublattices A and B become equivalent in the PM phase, where the fermion spectrum in Eq. (16) simplifies to

$$\hat{H}_f = -\chi_f^\text{v} \sum_{\mathbf{k},\sigma} \eta_\mathbf{k} f_{\mathbf{k}\sigma}^\dagger f_{\mathbf{k}\sigma}. \tag{18}$$

Here, the sum over $\mathbf{k}$ runs over the first Brillouin zone corresponding to a unit cell containing only one site.

2. Boson spectrum

The charged boson spectrum is governed by

$$\hat{H}_d = \sum_\mathbf{k} \Psi_\mathbf{k}^\dagger M_\mathbf{k} \Psi_\mathbf{k}, \quad \Psi_\mathbf{k} = [d_{A\mathbf{k}}, d_{B\mathbf{k}}, e_{B\bar{\mathbf{k}}}^\dagger, e_{A\bar{\mathbf{k}}}^\dagger]^T,$$

where the boson Hamiltonian matrix

$$M_\mathbf{k} = \begin{bmatrix} \epsilon_d^\text{v} + \lambda & -\chi_d^\text{v} \eta_\mathbf{k} & -\Delta_d^\text{v} \eta_\mathbf{k} & 0 \\ -\chi_d^\text{v} \eta_\mathbf{k}^* & \epsilon_d^\text{v} + \lambda & 0 & -\Delta_d^\text{v} \eta_\mathbf{k}^* \\ -\Delta_d^\text{v} \eta_\mathbf{k}^* & 0 & \epsilon_d^\text{v} + \lambda & -\chi_d^\text{v} \eta_\mathbf{k}^* \\ 0 & -\Delta_d^\text{v} \eta_\mathbf{k} & -\chi_d^\text{v} \eta_\mathbf{k} & \epsilon_d^\text{v} + \lambda \end{bmatrix}. \tag{19}$$

Here the relations due to the particle-hole symmetry at half-filling have been applied. Note that $M_{\mathbf{k}}$ is independent of spin. The boson dispersion is obtained by diagonalizing Eq. (19) using the standard boson Bogoliubov transformation:

$$E^d_{\pm}(\mathbf{k}) = \sqrt{\left(\epsilon^{\mathrm{v}}_{\mathbf{d}} + \lambda \pm \left|\chi^{\mathrm{v}}_{\mathbf{d}}\eta_{\mathbf{k}}\right|\right)^2 - \left|\Delta^{\mathrm{v}}_{\mathbf{d}}\eta_{\mathbf{k}}\right|^2}. \tag{20}$$

Each branch of the above dispersion is doubly degenerate. The condition for a real physical dispersion requires that $\epsilon^{\mathrm{v}}_d + \lambda \geqslant \zeta(|\chi^{\mathrm{v}}_d| + |\Delta^{\mathrm{v}}_d|)$. When the equality is satisfied, the boson spectrum is gapless and the bosons can condense into the zero-energy state. Otherwise, an energy gap,

$$\Xi_d = 2\sqrt{\left(\epsilon^{\mathrm{v}}_d + \lambda - \zeta\left|\chi^{\mathrm{v}}_d\right|\right)^2 - \left(\zeta\left|\Delta^{\mathrm{v}}_d\right|\right)^2},$$

develops in the boson spectrum and the doublon and holon condensate will be depleted.

In the PM phase on the square lattice, sublattices A and B become equivalent and the boson Hamiltonian matrix in Eq. (19) simplifies to

$$\hat{H}_d = \sum_{\mathbf{k},\sigma} \begin{bmatrix} d_{\mathbf{k}} \\ e^{\dagger}_{\bar{\mathbf{k}}} \end{bmatrix}^{\dagger} \begin{bmatrix} \epsilon^{\mathrm{v}}_d + \lambda - \chi^{\mathrm{v}}_d\eta_{\mathbf{k}} & -\Delta^{\mathrm{v}}_d\eta_{\mathbf{k}} \\ -\Delta^{\mathrm{v}}_d\eta_{\mathbf{k}} & \epsilon^{\mathrm{v}}_d + \lambda - \chi^{\mathrm{v}}_d\eta_{\mathbf{k}} \end{bmatrix} \begin{bmatrix} d_{\mathbf{k}} \\ e^{\dagger}_{\bar{\mathbf{k}}} \end{bmatrix}. \tag{21}$$

This results in a doubly degenerate boson dispersion relation:

$$E^d(\mathbf{k}) = \sqrt{\left(\epsilon^{\mathrm{v}}_{\mathbf{d}} + \lambda - \chi^{\mathrm{v}}_{\mathbf{d}}\eta_{\mathbf{k}}\right)^2 - \left(\Delta^{\mathrm{v}}_{\mathbf{d}}\eta_{\mathbf{k}}\right)^2}. \tag{22}$$

3. Self-consistency equations

The D-H binding saddle-point solution can be obtained by solving the set of self-consistency equations derived from minimizing the energy with respect to the variables $\{\chi_d, \Delta_d, n_d, p_{0\sigma}, \varepsilon, \lambda, \chi^{\mathrm{v}}_d, \Delta^{\mathrm{v}}_d, \epsilon^{\mathrm{v}}_d\}$:

$$\chi^{\mathrm{v}}_d = 2tgp_{0\uparrow}p_{0\downarrow}\chi_f, \tag{23}$$

$$\Delta^{\mathrm{v}}_d = g\chi_f \sum_{\sigma}\left(tp^2_{0\sigma} - g\Delta_d\chi^{\mathrm{v}}_f Y_{\sigma}\right), \tag{24}$$

$$\epsilon^{\mathrm{v}}_d = -\zeta g^2\chi_f\chi^{\mathrm{v}}_f \sum_{\sigma}\left(1 - p^2_{0\bar{\sigma}}\right)Y_{\sigma}, \tag{25}$$

$$p_{0\sigma} = \frac{2\zeta tg\chi_f(\chi_d p_{0\bar{\sigma}} + \Delta_d p_{0\sigma})}{\lambda - \lambda_{\sigma} - 2\zeta g^2\chi_f\chi^{\mathrm{v}}_f Y_{\bar{\sigma}}\left(1 - n_d - p^2_{0\sigma}\right)}, \tag{26}$$

$$p^2_{0\uparrow} - p^2_{0\downarrow} = n^f_{\uparrow} - n^f_{\downarrow}, \tag{27}$$

$$2n_d + p^2_{0\uparrow} + p^2_{0\downarrow} = 1, \tag{28}$$

$$\chi_d = d^2_0 + \frac{1}{2N\zeta}{\sum_{\mathbf{k}}}'\langle\eta_{\mathbf{k}}d^{\dagger}_{A\mathbf{k}}d_{B\mathbf{k}} + \mathrm{H.c.}\rangle, \tag{29}$$

$$\Delta_d = d^2_0 + \frac{1}{2N\zeta}{\sum_{\mathbf{k}}}'\langle\eta^*_{\mathbf{k}}d_{A\mathbf{k}}e_{B\bar{\mathbf{k}}} + \mathrm{H.c.}\rangle, \tag{30}$$

$$n_d = d^2_0 + \frac{1}{2N}\sum_{\alpha=\{A,B\}}{\sum_{\mathbf{k}}}'\langle d_{\alpha\mathbf{k}}d_{\alpha\mathbf{k}}\rangle, \tag{31}$$

where the fermion density n^f_{σ} and hopping χ_f per spin are readily obtained from the fermion spectrum in Eq. (16). It is instructive to examine the last three equations for the D/H hopping, the D-H binding, and the D/H density. The closing of the boson gap Ξ_d leads to a zero-energy mode at $\mathbf{k} = \mathbf{0}$ whose occupation enables the single-boson condensate $d^2_0 = e^2_0$. This zero mode will be subsequently taken out of the momentum summations in Eqs. (29)–(31). Accordingly, the solutions to this set of self-consistency, Eqs. (23)–(31), must be searched under two conditions: (i) assume $d_0 = 0$ and (ii) assume a nonzero d_0. In the latter case, one more variable, (d_0), is introduced together with one extra equation that ensures the existence of the zero-energy mode:

$$\epsilon^{\mathrm{v}}_d + \lambda = \zeta\left(\left|\chi^{\mathrm{v}}_d\right| + \left|\Delta^{\mathrm{v}}_d\right|\right). \tag{32}$$

If multiple solutions are found, the one with the lowest energy should be chosen as the ground state. In practice, we found only one solution at any given U.

4. Electron spectral function and spectral density

Once the saddle-point solution is obtained, the spectral function of the physical electrons can be calculated from the one-particle Green's function, $G_{\alpha\sigma}(\mathbf{k},\tau) = -\langle\mathbf{T}_{\tau}\mathbf{c}_{\alpha\mathbf{k}\sigma}(\tau)\mathbf{c}^{\dagger}_{\alpha\mathbf{k}\sigma}(\mathbf{0})\rangle$. The detailed derivation of the spectral function and the integrated spectral function (ISF), i.e., the tunneling density of states,

$$N_{\alpha}(\omega) = -\mathrm{Im}\int_0^{\beta} d\tau e^{i\omega\tau}\sum_{\mathbf{k},\sigma}G_{\alpha\sigma}(\mathbf{k},\tau), \tag{33}$$

are given in the Appendix. Note that since the spectral function involves convolutions of the (d,e) boson normal and the anomalous (due to pairing) Green's functions with those of the f_{σ} fermion, the single-particle energy gap for the physical electron is the sum of the fermion and boson gaps $\Xi = \Xi_d + \Xi_f$. More importantly, the coherent QP excitations would only emerge with the D/H condensate, which recombines the charge and spin degrees of freedom and can be detected by the QP coherent peaks in $N(\omega)$.

C. Ground-state wave functions

Before presenting the results on the honeycomb and the square lattice, it is instructive to discuss the possible phase structure in terms of the general form of the ground-state wave function of the D-H binding saddle point. Since the Hilbert space is represented by those of the fermion and the slave bosons, the electron ground-state wave function is a product of the ground-state wave functions for the bosons and fermions:

$$\Psi(\vec{r}_1\sigma_1,\ldots,\vec{r}_N\sigma_N) = \Psi_B(\vec{r}_1,\ldots,\vec{r}_{N_d};\vec{r}_1,\ldots,\vec{r}_{N_e}) \otimes \Psi_F(\vec{r}_1\sigma_1,\ldots,\vec{r}_N\sigma_N). \tag{34}$$

Here $\sigma_i, i = 1,\ldots,N$ labels the spins of N electrons, while N_d and N_e are the number of doublons and holons, respectively. From Eq. (16), it is clear that the fermion wave function is given by a Slater determinant, i.e., $\Psi_F = \Psi_{\mathrm{Slater}}(\{\vec{r}_i\sigma_i\})$ in both the PM- and the AF-ordered phases. Compared to the conventional wave-function form for an interacting many-body electron

system, $\Psi(\{\vec{r}_i\sigma_i\}) = \prod_{i<j} J(\vec{r}_i - \vec{r}_j)\Psi_{\rm Slater}(\{\vec{r}_i\sigma_i\})$, the variational Jastrow factor J has been promoted to full-fledged boson wave functions, thus allowing possible new electronic phases. The key physics in our theory is the boson intersite correlation. The corresponding boson ground-state wave function in second quantized form is thus a direct product of single-boson condensates and the pairing of uncondensed doublons and holons [33]. On the square lattice, the boson wave function from the Hamiltonian in Eq. (21) thus takes the form

$$|\Psi_B\rangle = (e_0^\dagger)^{N_e^0}(d_0^\dagger)^{N_d^0}|0\rangle_B \otimes \prod_{\mathbf{k}} \exp(-g_{\mathbf{k}} d_{\mathbf{k}}^\dagger e_{\bar{\mathbf{k}}}^\dagger)|0\rangle_B, \qquad (35)$$

where $|0\rangle_B$ is the vacuum of the boson sector, and the pairing function $g_{\mathbf{k}} = [\epsilon_d^{\rm v} + \lambda - \chi_d^{\rm v}\eta_{\mathbf{k}} - E^d(\mathbf{k})]/\Delta_{\mathbf{d}}^{\rm v}\eta_{\mathbf{k}}^*$. The boson wave function on the honeycomb lattice described by the Hamiltonian in Eq. (19) has a similar, slightly more complicated form due to the doubling of the unit cell. In the first part of the boson wave function, N_e^0 and N_d^0 are the numbers of condensed holons and doublons that are determined by the condensate density $e_0^\dagger e_0$ and $d_0^\dagger d_0$. This is the only part retained in the KR saddle point or the Gutzwiller approximation. Together with Ψ_F, they describe the coherent QP part in the excitation spectrum of a correlated Fermi fluid. The second part is due to D-H binding, which, together with Ψ_F, describes the incoherent excitations and plays an integral part in the Mott transition. As long as the condensate part is present, the charge and spin degrees of freedom combine such that the elementary excitations carry the quantum numbers of an electron and appear as QP poles in the single-particle Green's function. Thus, the coexistence of the condensate and the binding parts heralds the coherent QP and the incoherent Hubbard excitations in Mott-Hubbard systems before the Mott transition. This is the case in both the PM ($U < U_{c1}$) and the Slater AF ($U_{c1} < U < U_{c2}$) phase, where $N_e^0 = N_d^0 \neq 0$ in the condensed part of the boson wave function Ψ_B, while Ψ_F changes from a PM to an AF Slater determinant. However, as we will show, when $U > U_{c2}$, the quantum fluctuations due to D-H binding destroy the single-particle condensate, i.e., $N_e^0 = N_d^0 = 0$, as all doublons and holons are bound together, giving rise to a charge gap. The boson wave function is given entirely by the second part in Eq. (35). Interestingly, this boson wave function is just the wave function of a resonating valence bond (liquid) state, which in the present context can also be understood as that of an excitonic insulator, since the doublon and holon carry opposite charges. Because all the doublons are bound to the holons, the elementary excitations do not carry the quantum numbers of an electron and the entire single-particle excitations are incoheren,t as the charge and spin cannot recombine to form a coherent QP. Had this Mott transition taken place before the AF order, this insulating phase would be an SL. However, as we will see on bipartite lattices without frustration, AF order happens before the Mott transition, i.e., $U_{c2} > U_{c1}$. We thus term the phase for $U > U_{c2}$ the AF* phase, which is indeed an example of spin-charge separation above one dimension, albeit taking place inside the AF-ordered phase. Note that what distinguishes the AF* phase from the Slater AF insulator is the complete depletion of the single-particle condensates of the holons and doublons above U_{c2} such that all doublons are bound to holons.

D. Mott, Slater AF, and AF Mott transitions

1. Results on the honeycomb lattice

The D-H binding saddle-point solutions on a half-filled honeycomb lattice are summarized in Figs. 4 and 5. The variational parameters $\chi_d^{\rm v}$ and $\Delta_d^{\rm v}$ and the order parameters for D/H hopping χ_d and D-H pairing Δ_d are plotted in Figs. 4(a) and 4(b) as functions of the Hubbard U. At $U = 0$, $\Delta_d^{\rm v} = 0$, thus all doublons and holons are single particle condensed with $d_0^2 = e_0^2 = p_{0\sigma}^2 = 1/4$ such that $\chi_f^{\rm v} = t$, recovering the noninteracting limit. The SM phase remains stable at small U. With increasing U, the doublon density decreases as shown in Fig. 4(c). Due to the increase in D-H binding, the D/H condensate d_0 decays more rapidly than in the KR saddle-point solution shown in Fig. 2(a). To study the Mott transition, we first restrict the solution to be in the PM phase by enforcing $p_{0\uparrow} = p_{0\downarrow}$, which amounts to suppressing possible magnetically ordered states. As shown in Fig. 4(c), the Mott transition takes place at $U_c \simeq 7.3t$, which is considerably smaller than that of $12.6t$ for the BR transition [Fig. 2(a)]. The condensate d_0 vanishes and all doublons are bound with the holons in the Mott insulating phase for $U > U_c$, accompanied by the opening of a charge gap Ξ_d that is linear in $U - U_c$ [Fig. 4(d)]. The ISF of the physical electrons is shown in Fig. 5(a). Note the transfer of the coherent QP weight to the incoherent part with increasing U and the complete suppression of the coherent QPs in favor of two broad incoherent spectral features beyond the Mott transition that originate from the bosonic excitations $E_\pm^d(\mathbf{k})$ in Eq. (19) to be discussed later. Since the $f_{i\sigma}$-fermion spinon remains gapless, the insulating phase is a gapless SL. Thus, we find no evidence of the honeycomb lattice for the proposed gapped SL phase [6].

Next, we allow magnetism and study the interplay among AF order, D-H binding, and the Mott transition in the ground state. Figure 4(c) shows that the SM phase on the honeycomb lattice remains stable until a critical $U_{c1} \simeq 3.4t$, where the staggered magnetization (m) onsets. We find that for $U_{c1} < U < U_{c2}$, where $U_{c2} \simeq 5.7t$, although a single-particle gap Ξ_f opens in the fermion sector [Fig. 4(d)], the zero-energy mode remains stable in the d-e sector and continues to support the D/H condensate. Thus, the spin and charge continue to recombine in this regime and there are coherent excitations corresponding to the sharp QP peaks in the ISF shown in Fig. 5(b) at $U = 4t$ and $5t$. This phase is thus an Slater AF insulator whose wave function would overlap well with an AF Slater determinant.

Remarkably, a Mott transition in the presence of AF order takes place at U_{c2}. For $U > U_{c2}$, an AF Mott phase (i.e., the AF* phase) emerges with the opening of the boson gap $\Xi_d \propto U - U_{c2}$ in the d-e sector [Fig. 4(d)] as the D/H condensate vanishes. Since all doublons are bound to holons, the charge and spin cannot recombine and the electrons are thus fractionalized in the AF* phase. A direct consequence of the lack of elemental excitations carrying the electron quantum number is the lack of coherent QP peaks in an entirely incoherent excitation spectrum, as can be seen from the broad ISF at $U > U_{c2}$ in Fig. 5(b) at $U = 6t$ and $7t$. Unlike in the Slater AF phase, the vanishing of the D/H condensate in the AF* phase enables the deconfinement of the

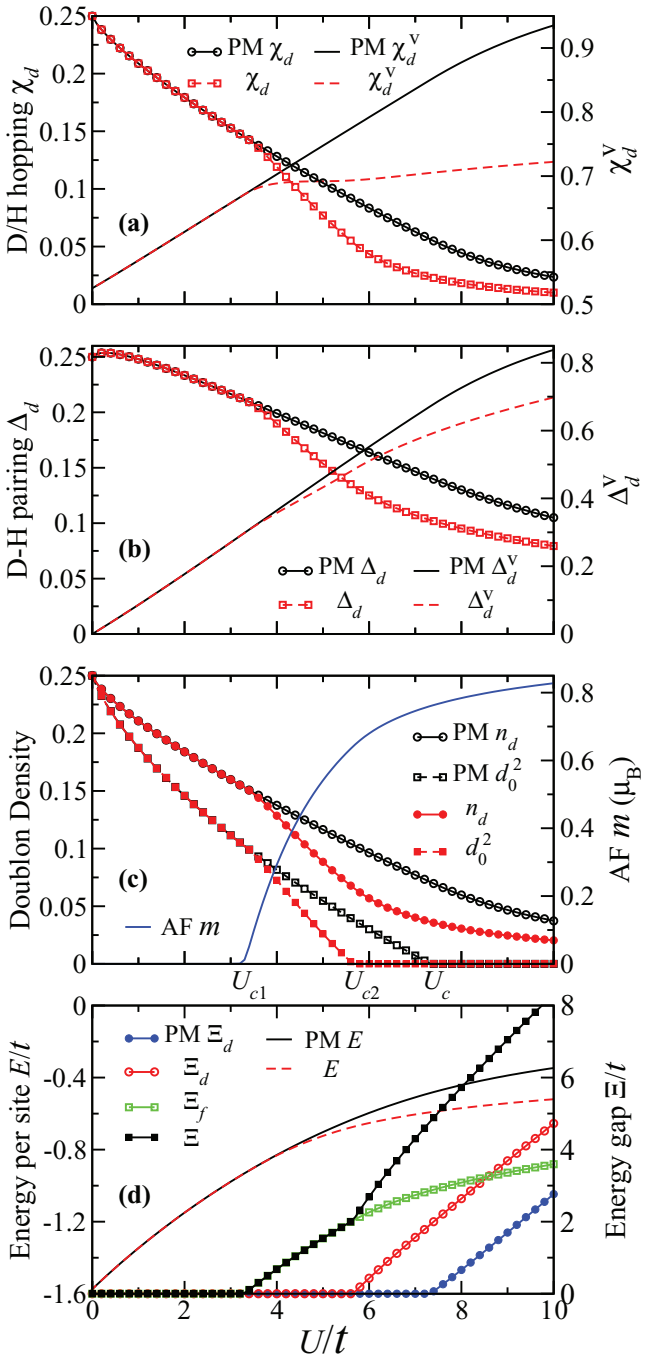

FIG. 4. (Color online) D-H binding saddle-point solutions on a honeycomb lattice. The Hubbard U dependence of (a) variational parameters χ_d^v and D/H hopping order parameter χ_d; (b) variational parameter Δ_d^v and D-H pairing order parameter Δ_d; (c) D/H density n_d, condensate density d_0^2, and AF staggered magnetization m; and (d) ground-state energy per site E and energy gaps in the boson sector Ξ_d, the fermion sector Ξ_f, and for the physical electrons $\Xi = \Xi_f + \Xi_d$. Corresponding results in the restricted PM phase are also shown. In the restricted PM phase, the Mott transition (SM to Mott insulator) takes place at $U_c \simeq 7.3t$, while the ground state undergoes two transitions: the magnetic transition (from SM to Slater AF insulator) at $U_{c1} \simeq 3.4t$ and the Mott transition (from Slater AF to AF* phase) at $U_{c2} \simeq 5.7t$.

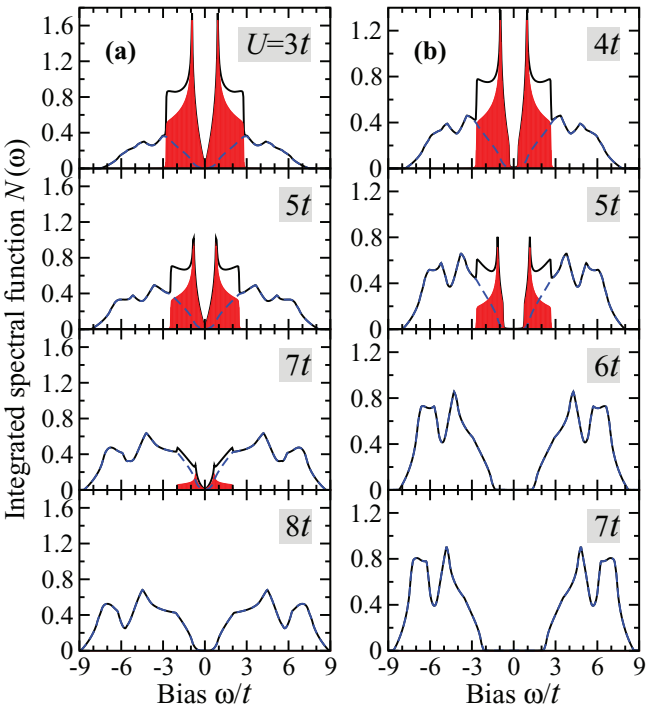

FIG. 5. (Color online) Integrated spectral function (ISF) with D-H binding on the honeycomb lattice. The coherent [shaded (red) areas], incoherent [lighter solid (blue) lines], and total (solid black lines) ISF at different values of Hubbard U in (a) the restricted PM phase, where the Mott transition is at $U_c \simeq 7.3t$, and (b) the ground state, where the AF-to-AF* transition is at $U_{c2} \simeq 5.7t$.

spin and charge degrees of freedom, such that the ground wave function has no overlap with Slater determinant-like states. The excitation energy gap for the physical electron, $\Xi = \Xi_f + \Xi_d$, exhibits a derivative discontinuity at U_{c2} [Fig. 4(d)] due to the opening of the Mott gap Ξ_d in the AF* phase. However, the magnetization m remains analytic across the AF $\rightarrow$ AF* transition in Fig. 4(c), which is a topological confinement-deconfinement transition associated with the Ising-like global Z_2 symmetry ($d_i \rightarrow -d_i$, $e_i \rightarrow -e_i$), which is broken in the Slater AF phase by the D/H condensate and restored in the AF* phase.

The continuous SM-to-AF transition at $U_{c1} \simeq 3.4t$ compares well to the most recent QMC calculations on large system sizes by Sorella *et al.* [12], which find the onset of AF order and a single-particle excitation gap at $U \simeq 3.8t$. Since we have not included the intersite spin fluctuations described by the dynamics of the p_σ boson, our magnetic gap is somewhat larger than the QMC values, and we do not attempt quantitative comparisons to results obtained by other numerical methods such as cluster dynamical mean-field theory (CDMFT) calculations with continuous-time QMC (CTQMC) or ED impurity solvers. While the CTQMC-CDMFT [7,11] is performed at relative high temperatures and is not very suitable for extracting small energy gaps in the quantum states, the ED-CDMFT [8,9] as well as the ED-VCA (variational cluster approximation) [10,13] revealed spurious excitation gaps at very small U, before the emergence of AF order. This was viewed as supporting evidence for the proposed

gapped SL phase [6]. Recently, Hassan and Sénéchal [14] noted that these ED-CDMFT and ED-VCA calculations use only a single bath orbital per cluster site, which they argued is insufficient and leads to artificial excitation energy gaps for all nonzero values of U. Their calculations with two bath orbitals connecting each cluster site show that the PM Mott transition and thus the SL phase are indeed pre-empted by a magnetic transition occurring at a lower value of U. Liebsch and Wu [15] further pointed out that the spurious excitation gap at very small U originates from the breaking of the translation symmetry in these cluster calculations.

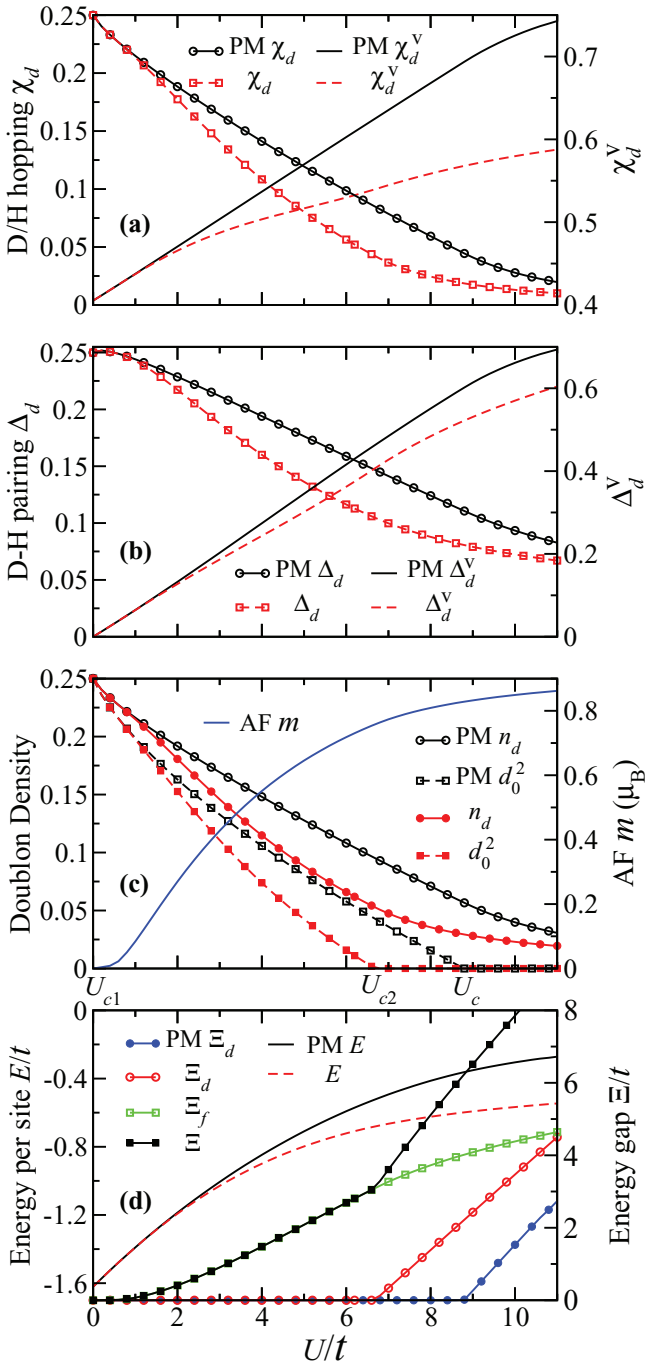

FIG. 6. (Color online) D-H binding saddle-point solutions on a square lattice, where $U_c \simeq 8.8t$, $U_{c1} = 0$, and $U_{c2} \simeq 6.8t$. Labels and notations follow those in Fig. 4.

2. *Results on the square lattice*

Figures 6 and 7 show the results obtained on the half-filled square lattice, which are qualitatively the same as those obtained on the honeycomb lattice. In the PM phase, the Mott transition is at $U_c \simeq 8.8t$ in contrast to the BR transition at $U_{BR} \simeq 13t$ without taking D-H binding into account. Because the band structure leads to a perfectly nested Fermi surface at half-filling, the PM metallic phase is unstable towards AF order for infinitesimal U on the square lattice. The AF order therefore emerges at $U_{c1} = 0$ with an exponentially small staggered magnetization, as shown in Fig. 6(c). This Slater AF insulator with coherent QP excitations is stable until $U_{c2} \simeq 6.8t$, where a transition into the AF* phase with the vanishing of the holon/doublon condensate and the opening of the charge gap [Figs. 6(c) and 6(d)] and the disappearance of coherent QP peaks in favor of two broad incoherent features in the integrated spectral density Fig. 7. It is important to note that the Fermi level density of states, whose two limiting behaviors, vanishing or divergent, are presented by the unfrustrated honeycomb and square lattices, respectively, while affecting the PM to Slater AF transition, does not play an essential role in determining the Mott transition from the Slater AF to the AF* phase. This is because the latter is tied to the opening of the charge gap in the boson sector near the doublon and holon band bottom above a finite U_{c2}, as can be seen from the boson dispersions shown in Fig. 9.

To further explore the generality of these predictions, we have studied the case where the noninteracting band has a

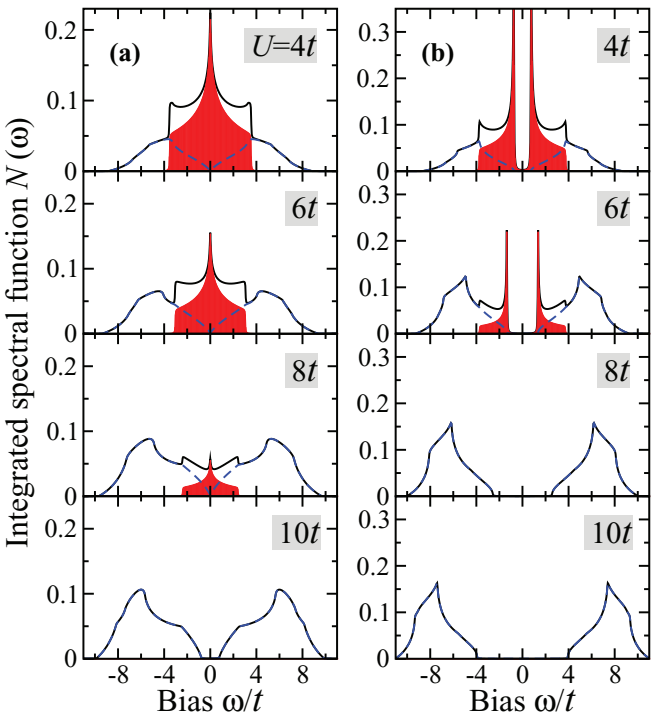

FIG. 7. (Color online) ISF with D-H binding on the square lattice. Labels and notations follow those in Fig. 5.

semicircular density of state, $\rho(\omega) = (4/\pi W)\sqrt{1-(2\omega/W)^2}$, where W is the bandwidth. We found an identical phase structure with a PM metal to Slater AF insulator at $U_{c1} \simeq 0.1W$, followed by the Mott transition to that AF* phase at $U_{c2} \simeq W$. Note that although the semicircle density of states can be realized in the infinite-d unfrustrated Bethe lattice, these results should not be considered as obtained for the infinite-d Hubbard model, since taking the infinite-d limit would suppress all intersite correlations, including the intersite D-H binding considered here. Thus, in the infinite-d limit, we would only recover the KR saddle-point solution, i.e., the Gutzwiller approximation, which is exact for the Gutzwiller wave-function approach in infinite dimensions [32]. In this sense, our approach can be viewed as going beyond the Gutzwiller approximation by including the intersite correlations in physical dimensions.

With this difference in mind, we proceed to compare in Fig. 8 the local spectral function in the PM phase on the square lattice of our D-H binding theory with the results obtained from the single-site DMFT on the square lattice [34] at different Hubbard U values. Overall, we find remarkable agreement in the incoherent part of the spectrum for all values of U/t on both sides of the Mott transition. The most significant deviations of the results are in the low-energy QP peaks around the Mott transition. The main cause of the latter can be traced to a particular property of the single-site DMFT formulation that the spectral density at $\omega = 0$ is independent of U in the infinite-d limit of the Hubbard model [35], which holds the QP peak at a constant height until its width goes to 0 at the Mott transition, shown by the DMFT data in Fig. 8. The latter is no longer true in the presence of intersite correlations beyond the infinite-d limit, as shown in the D-H binding results in Fig. 8, where the QP peaks, agreeing with the DFMT result for moderate U, are suppressed in both height and width and disappear completely at the Mott transition, whose critical value is significantly reduced by intersite correlations [36]. We also find broad qualitative agreement with the local spectral density of cluster DMFT calculations that captures certain short-range correlations, although finding consistency in CDMFT results is difficult due to the different cluster embedding procedure (including cluster shapes and sizes) and the choice of the impurity solver. We find that it is particularly intriguing that in the CDMFT study of the PM phase by Park *et al.* [36], the metallic phase has an ISF consistent with our result in the PM phase, whereas on the insulating side near the metal-insulator transition, the local spectral function displayed a small gap with very pronounced peaks at the gap edge that closely resemble our findings in the AF Slater insulator. Indeed, these peaks at the edge of the magnetic gap are a clear hallmark of the coherence QP peaks characteristic of a Slater spin-density wave insulator. We thus conjecture that the CDMFT findings of a small gap PM insulating state with pronounced gap-edge coherence peaks are due to the fluctuating or short-range Slater AF order, and with increasing U, a true Mott transition would emerge with the suppression of the QP peaks and the opening of the charge gap.

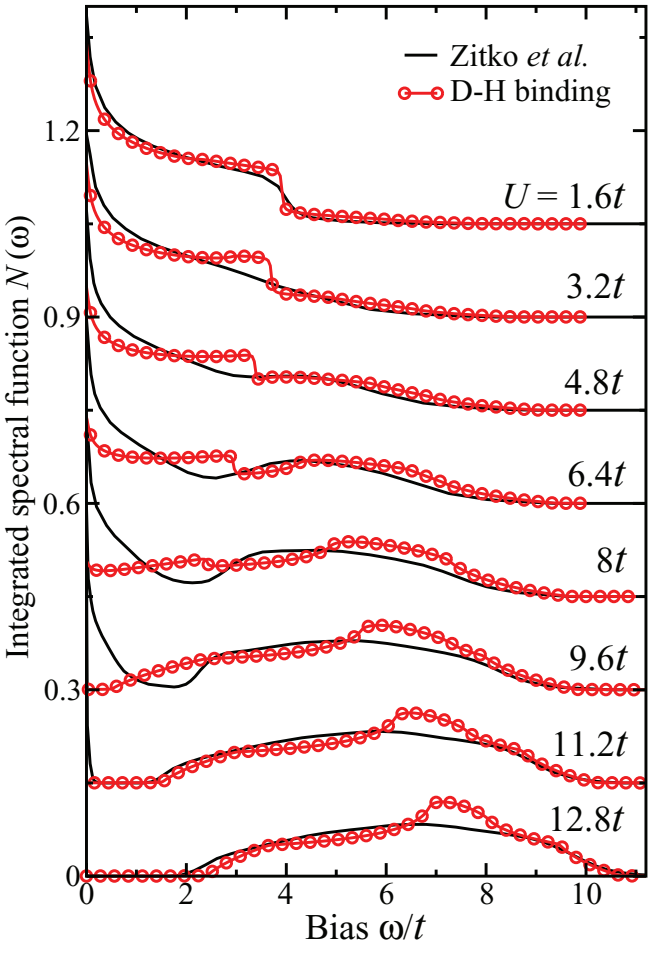

FIG. 8. (Color online) Local spectral function obtained from the D-H binding theory and the single-site DMFT by Žitko *et al.* [34] on a paramagnetic square lattice at various U. Curves are offset vertically for clarity.

3. *Stability of the D-H binding saddle point*

Next we comment on the D-H binding saddle-point stability with respect to gauge-field fluctuations. It is known that the KR formulation introduces three $U(1)$ gauge fields [37] since the action is invariant under $e_i \to e_i e^{i\theta_i}$, $p_{i\sigma} \to p_{i\sigma} e^{i\phi_{i\sigma}}$, $d_i \to d_i e^{-i\theta_i + i\sum_\sigma \phi_{i\sigma}}$, $f_{i\sigma} \to f_{i\sigma} e^{i\theta_i - i\phi_{i\sigma}}$, and $\lambda_i \to \lambda_i + \dot{\theta}_i$, $\lambda_{i\sigma} \to \lambda_{i\sigma} + \dot{\theta}_i - \dot{\phi}_{i\sigma}$. The $p_{i\sigma}$ condensate breaks two of the $U(1)$ symmetries and makes the gauge fields associated with $\phi_{i\sigma}$ massive by the Anderson-Higgs mechanism. The remaining $U(1)$ symmetry is also broken in the SM and the AF phase by the D/H condensate, making the θ_i gauge field massive. In the AF* phase, it is the D-H pairing Δ_{ij} that breaks the $U(1)$ symmetry and the θ_i gauge field remains massive, as does its staggered component due to the D/H hopping fields $\chi_{ij}^{d,e}$. The absence of gapless gauge-field fluctuations supports the stability of the obtained phases.

E. Nature of incoherent Mott-Hubbard excitations

It is enlightening to discuss the energy spectrum and the spectral function of the doublons and holons in connection to the nature of the incoherent Mott-Hubbard excitations in the local spectral function. The dispersion of the holons and doublons in Eqs. (20) and (22) and the corresponding density of

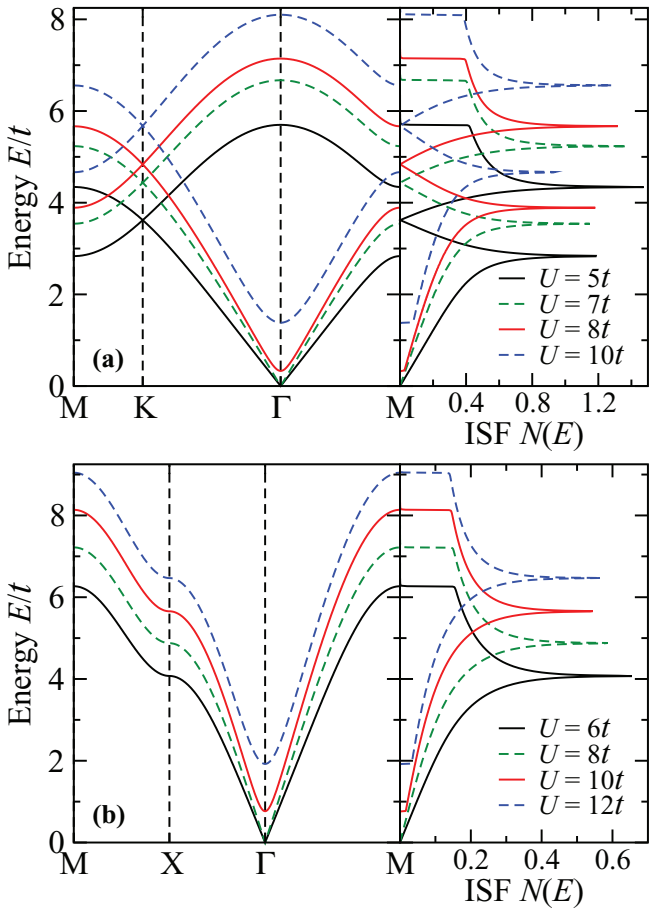

FIG. 9. (Color online) Energy spectrum along high-symmetry directions (left) and ISF (right) of doublons and holons in the restricted PM phases at several Hubbard U values across the Mott transition on (a) a honeycomb lattice where $U_c \simeq 7.3t$ and (b) a square lattice where $U_c \simeq 8.8t$. The single-particle condensate contribution to the ISF (a δ function at zero energy) on the metallic side of the Mott transition is not shown.

states are shown in Fig. 9 in the PM phases of the honeycomb and square lattice Hubbard models, respectively, at several values of U across the Mott transition. Their behaviors are similar in the AF and AF* phases.

1. Honeycomb lattice

At a fixed U, the boson spectrum shows two doubly degenerate dispersive branches given in Eq. (20). There are several noteworthy features. (i) Both dispersive branches are flat near the M point of the hexagonal Brillouin zone, leading to the two Van Hove singularities in the boson ISF plotted in the right panel in Fig. 9(a). (ii) The two branches cross and produce the Dirac cone at the high-symmetry K point at a finite energy that increases with increasing U, leading to the V-shaped density of states. Remarkably, (i) and (ii) combine to form a Dirac-cone like dispersion that is similar and can be regarded as a "ghost" band of the bare electron dispersion carried by the excitations of the D/H complex. This property was pointed out in a systematic large-N expansion study of the t-J model for doped Mott insulators [38]. It is remarkable that the ghost Dirac-cone feature manifests itself in the broad peak-dip-peak structure in the incoherent part of the ISF for the physical electrons shown in Fig. 5(a), which can now be identified as D-H excitations. (iii) The low-energy properties of the boson dispersion near the Γ point is also intriguing. For $U < U_c$, i.e., on the metallic side of the Mott transition, the lower energy branch is gapless, i.e., $E^d_-(\mathbf{k}) = \mathbf{0}$, and disperses linearly away from the Γ point. The existence of the zero-energy mode, together with the vanishing of the ISF $N(E)$, enables finite-temperature D/H condensation in a two-dimensional system such that $d_0 \neq 0$ at zero temperature. In contrast, for $U > U_c$, or $U > U_{c2}$ when magnetism is allowed, a charge gap $\Xi_d \neq 0$ opens up at the Γ point, indicating the emergence of the Mott insulating or the AF* phase with complete suppression of the D/H condensate. Note also that the gapped $E^d_-(\mathbf{k})$ is parabolic near Γ, giving rise to a finite ISF $N(E)$ at the band bottom.

2. Square lattice

The above findings on the connection between the incoherent Mott-Hubbard excitations and the doublon-holon spectrum applies in a straightforward manner to the square lattice case as well. In contrast to the intrinsic two-sublattice structure of the honeycomb lattice, the boson spectrum on the square lattice has only one branch given in Eq. (22), which is shown in Fig. 9(b). The corresponding density of states has a single Van Hove peak tied to the dispersion near the X point. Similarly to the honeycomb lattice case, this branch of D-H excitations manifests itself in the single broad peak on the particle and the hole side of the electron local spectral function shown in Fig. 7.

The change in the bosonic dispersion across the AF Mott transition, i.e., from the Slater AF insulator to the AF* phase, is qualitatively the same as those displayed in Fig. 9 for the PM Mott transition. Namely, the boson spectrum is gapless with a linear dispersion supported by the D/H single-particle condensate on the Slater AF side and develops an energy gap, when all holons are bound to doublons, above which a quadratic dispersion is found for the Bogoliubov quasiparticles. The linear dispersion in the PM phase is a bosonic representation of the collective zero-sound excitations in the Landau Fermi liquid. In the Slater AF phase, despite the opening of a single-particle magnetic gap, the absence of a charge gap is reflected in the existence of gapless collective excitations represented by the bosons. It is only after entering the AF* phase that the charge excitations are gapped out, leaving only the spin waves as the low-energy excitations inside the single-particle energy gap.

IV. CONCLUSIONS

In summary, we have shown that binding between doublons and holons plays an essential role in describing the incoherent excitations and the Mott transition in strongly correlated Mott-Hubbard systems. For the honeycomb lattice Hubbard model, we have shown that the SM–to–AF Slater insulator transition is followed by a Mott transition into a fractionalized AF* phase with increasing U. Interestingly, a different AF* phase of a fractionalized antiferromagnet was proposed in the effective

Z_2 gauge theory description of doped Mott insulators in the projected ($U = \infty$) Hilbert space where spinons are paired into a Néel state and doublons are absent [39]. In contrast, the incoherent charge excitation through D-H binding is essential in the AF* phase proposed here, which is more in line with the importance of doublons in describing Mottness emphasized recently [40].

The most practical way to test our predictions is to measure the energy gap for single-particle excitations using spectroscopic probes such as ARPES and STM. Our theory shows that with increasing U/W (which can be varied experimentally by applying pressure or isoelectronic chemical substitution), the system goes from a gapless PM state to an AF insulator where the single-particle gap is controlled by the magnetic gap, followed by a transition to the AF* phase where a charge gap opens and is added on top of the magnetic gap. Thus, there is a singularity (kink) in the evolution of the gap as a function of U/W. Perhaps even more directly, the single-particle spectral function as measured by ARPES shows well-defined QP peaks above the magnetic gap in the Slater AF phase but exhibits no coherent excitations in the AF* phase. Such an AF* phase on a square lattice may have been observed in the parent AF insulating compound of high-T_c cuprates by ARPES experiments [41], which find no coherent QP excitations at all energies.

As a concrete example, we propose to revisit the time-honored Mott-Hubbard system, i.e., the transition metal oxide V_2O_3, under chemical pressure achieved by Cr or Ti substitutions. In this case, a finite-temperature Mott metal-insulator transition above the low-temperature AF insulating ground state has been well established as a function of chemical substitution [42–44]. Our theory predicts that, hidden inside the AF insulating ground state, is a transition from a Slater AF to the AF* phase. Moreover, melting the AF order in the Slater AF insulator would result in a metallic state, whereas melting the AF* phase at higher Cr substitutions gives rise to a Mott insulator at finite temperatures. Performing the experiments described above in these materials would either provide support or disprove our theory.

ACKNOWLEDGMENTS

We thank F. Wang and Y. Yu for useful discussions. This work was supported by DOE Grant Nos. DE-FG02-99ER45747 and DE-SC0002554 and the Thousand Youth Talents Plan of China (S.Z.). Z.W. thanks the Aspen Center for Physics for their hospitality.

APPENDIX: ISF OF PHYSICAL ELECTRONS

The ISF, which equals the tunneling density of states, for the physical electrons is given by

$$N_\alpha(\omega) = -\sum_{\mathbf{k},\sigma} \mathrm{Im} \int_0^\beta d\tau e^{i\omega\tau} G_{\alpha\sigma}(\mathbf{k},\tau),$$

where the retarded single-particle Green's function [45]

$$G_{\alpha\sigma}(\mathbf{k},\tau) = -\langle \mathbf{T}_\tau \mathbf{c}_{\alpha\mathbf{k}\sigma}(\tau)\mathbf{c}^\dagger_{\alpha\mathbf{k}\sigma}(\mathbf{0})\rangle,$$

with α the sublattice index. In the KR slave-boson formulation [17], the electron operator is composed of $c_{i\sigma} = \hat{L}_{i\sigma}(e_i^\dagger p_{i\sigma} + p_{i\bar{\sigma}}^\dagger d_i)\hat{R}_{i\sigma} f_{i\sigma}$. Within our saddle-point solution, $\hat{L}_{i\sigma}$ and $\hat{R}_{i\sigma}$ are approximated by their saddle-point average for the local Green's functions. The electron operator in momentum space is thus given by

$$c_{\alpha\mathbf{k}\sigma} = r_{\alpha\sigma} \sum_{\mathbf{q},\mathbf{q}'} (e^\dagger_{\alpha\bar{\mathbf{q}}} p_{\alpha\mathbf{q}'\sigma} + p^\dagger_{\alpha\bar{\mathbf{q}}'\bar{\sigma}} d_{\mathbf{q}}) f_{\alpha,\mathbf{k}-\mathbf{q}-\mathbf{q}',\sigma},$$

with the normalization factor

$$r_{\alpha\sigma} = \langle \hat{L}_{\alpha\sigma}\hat{R}_{\alpha\sigma}\rangle = \left[\left(1 - n_d - p^2_{\alpha 0\sigma}\right)\left(1 - n_e - p^2_{\alpha 0\bar{\sigma}}\right)\right]^{-1/2}.$$

Therefore, the electron Green's function

$$G_{\alpha\sigma}(\mathbf{k},\tau) = \mathbf{r}^2_{\alpha\sigma} \sum_{\mathbf{q},\mathbf{q}'} \Lambda_{\alpha\sigma}(\mathbf{q},\mathbf{q}',\tau)\mathbf{G}^{\mathbf{f}}_{\alpha\sigma}(\mathbf{k}-\mathbf{q}-\mathbf{q}',\tau),$$

where $G^f_{\alpha\sigma}(\mathbf{k},\tau) = -\langle T_\tau f_{\alpha\mathbf{k}\sigma}(\tau) f^\dagger_{\alpha\mathbf{k}\sigma}(0)\rangle$ is the f_σ-fermion Green's function, which can be computed easily in terms of the fermionic QPs defined in Eq. (16), and Λ involves the normal and anomalous (due to pairing) Green's functions of the bosons,

$$\begin{aligned}\Lambda_{\alpha\sigma}(\mathbf{q},\mathbf{q}',\tau) = {} & \langle T_\tau e^\dagger_{\alpha\bar{\mathbf{q}}}(\tau) e_{\alpha\bar{\mathbf{q}}}(0)\rangle \langle T_\tau p_{\alpha\mathbf{q}'\sigma}(\tau) p^\dagger_{\alpha\mathbf{q}'\sigma}(0)\rangle \\ & + \langle T_\tau d_{\alpha\mathbf{q}}(\tau) d^\dagger_{\alpha\mathbf{q}}(0)\rangle \langle T_\tau p^\dagger_{\alpha\bar{\mathbf{q}}'\bar{\sigma}}(\tau) p_{\alpha\bar{\mathbf{q}}'\bar{\sigma}}(0)\rangle \\ & + \langle T_\tau e^\dagger_{\alpha\bar{\mathbf{q}}}(\tau) d^\dagger_{\alpha\mathbf{q}}(0)\rangle \langle T_\tau p_{\alpha\mathbf{q}'\sigma}(\tau) p_{\alpha\bar{\mathbf{q}}'\bar{\sigma}}(0)\rangle \\ & + \langle T_\tau d_{\alpha\mathbf{q}}(\tau) e_{\alpha\bar{\mathbf{q}}}(0)\rangle \langle T_\tau p^\dagger_{\alpha\bar{\mathbf{q}}'\bar{\sigma}}(\tau) p^\dagger_{\alpha\mathbf{q}'\sigma}(0)\rangle.\end{aligned}$$

The ISF of the physical electrons becomes

$$N_\alpha(\omega) = -\sum_{\mathbf{k},\sigma} r^2_{\alpha\sigma} \mathrm{Im} \int_0^\beta d\tau e^{i\omega\tau} \Lambda_{\alpha\sigma}(\tau) G^f_{\alpha\sigma}(\mathbf{k},\tau), \quad \text{(A1)}$$

where $\Lambda_{\alpha\sigma}(\tau) = \sum_{\mathbf{q},\mathbf{q}'} \Lambda_{\alpha\sigma}(\mathbf{q},\mathbf{q}',\tau)$.

It is instructive to write each boson operator as the sum of the condensate and fluctuations: $b^{(\dagger)}_{\mathbf{k}} = b_0\delta_{\mathbf{k}} + \tilde{b}^{(\dagger)}_{\mathbf{k}}$, where b stands for the (d, e, p_σ) bosons. Although this is not necessary, doing so facilitates well the following discussion of the coherent and incoherent contributions to the electron spectral function. Note that the fluctuations $\tilde{b}^{(\dagger)}_{\mathbf{k}}$ are boson operators, obeying boson commutation relations and the energy spectrum discussed above. Thus, the normal and anomalous boson Green's functions can be written as

$$\langle T_\tau b^{(\dagger)}_{\mathbf{k}}(\tau) b'^{(\dagger)}_{\mathbf{q}}(0)\rangle = b_0 b'_0 \delta_{\mathbf{k}}\delta_{\mathbf{q}} + \langle T_\tau \tilde{b}^{(\dagger)}_{\mathbf{k}}(\tau)\tilde{b}'^{(\dagger)}_{\mathbf{q}}(0)\rangle.$$

Decomposing the condensate and fluctuation contributions this way and keeping the leading-order fluctuations involving a single boson Green's function, we have

$$\Lambda_{\alpha\sigma}(\tau) = \Lambda^{\mathrm{cond}}_{\alpha\sigma}(\tau) + \Lambda^{\mathrm{fluc}}_{\alpha\sigma}(\tau), \quad \text{(A2)}$$

where the condensate part

$$\Lambda^{\mathrm{cond}}_{\alpha\sigma}(\tau) = d_0^2(p_{0\uparrow} + p_{0\downarrow})^2, \quad \text{(A3)}$$

and the fluctuation part

$$\Lambda^{\rm fluc}_{\alpha\sigma}(\tau) = p^2_{\alpha 0\sigma}\sum_{\mathbf{q}}\langle T_\tau \tilde{e}^\dagger_{\alpha\bar{\mathbf{q}}}(\tau)\tilde{e}_{\alpha\bar{\mathbf{q}}}(0)\rangle + p^2_{\alpha 0\bar{\sigma}}\sum_{\mathbf{q}}\langle T_\tau \tilde{d}_{\alpha\mathbf{q}}(\tau)\tilde{d}^\dagger_{\alpha\mathbf{q}}(0)\rangle + d_0^2\sum_{\mathbf{q}}[\langle T_\tau \tilde{p}_{\alpha\mathbf{q}\sigma}(\tau)\tilde{p}^\dagger_{\alpha\mathbf{q}\sigma}(0)\rangle + \langle T_\tau \tilde{p}^\dagger_{\alpha\bar{\mathbf{q}}\bar{\sigma}}(\tau)\tilde{p}_{\alpha\bar{\mathbf{q}}\bar{\sigma}}(0)\rangle] + p_{0\uparrow}p_{0\downarrow}\sum_{\mathbf{q}}[\langle T_\tau \tilde{e}^\dagger_{\alpha\bar{\mathbf{q}}}(\tau)\tilde{d}^\dagger_{\alpha\mathbf{q}}(0)\rangle + \langle T_\tau \tilde{d}_{\alpha\mathbf{q}}(\tau)\tilde{e}_{\alpha\bar{\mathbf{q}}}(0)\rangle]. \quad \text{(A4)}$$

Correspondingly, the ISF in Eq. (A1) can be written as

$$N_\alpha(\omega) = N^{\rm coh}_\alpha(\omega) + N^{\rm incoh}_\alpha(\omega), \quad \text{(A5)}$$

with

$$N^{\rm coh(incoh)}_\alpha(\omega) = -\sum_{\mathbf{k},\sigma} r^2_{\alpha\sigma}\,{\rm Im}\int_0^\beta d\tau e^{i\omega\tau}\Lambda^{\rm cond(fluc)}_{\alpha\sigma}(\tau)G^f_{\alpha\sigma}(\mathbf{k},\tau). \quad \text{(A6)}$$

The coherent part of the ISF comes from the single-boson condensates that recombine the charge and spin degrees of freedom, leading to coherent QP excitations associated with the coherence peaks in the ISF. Beyond the Mott transition, the condensate of doublons and holons vanishes, and the coherent ISF is completely suppressed.

In the incoherent part of the ISF defined in Eq. (A6), the convolution of the boson and fermion Green's functions gives broad spectral features. Since the p_σ bosons are fully condensed and their fluctuations were ignored for simplicity within our D-H saddle-point solution, the question arises as to how to evaluate the corresponding Green's functions in Eq. (A4). Note that at the saddle-point level, the local constraint in Eq. (6) is only satisfied on average, i.e., $\langle \hat{Q}_{i\alpha}\rangle = 0$. When fluctuations are considered, a consistent condition imposed by the constraint is $\langle T_\tau \hat{Q}_\alpha(\tau)\hat{Q}_\alpha(0)\rangle = 0$, where $\hat{Q}_\alpha = (1/N)\sum_{i\in\alpha}\hat{Q}_{i\alpha}$, with N the number of α-sublattice sites. Evaluating the latter to the leading order in the boson correlations, one gets the following relation:

$$\frac{p^2_{0\uparrow}+p^2_{0\downarrow}}{2}\sum_{\mathbf{k}}[\langle T_\tau \tilde{p}^\dagger_{\alpha\bar{\mathbf{k}}\downarrow}(\tau)\tilde{p}_{\alpha\bar{\mathbf{k}}\downarrow}(0)\rangle + \langle T_\tau \tilde{p}_{\alpha\mathbf{k}\uparrow}(\tau)\tilde{p}^\dagger_{\alpha\mathbf{k}\uparrow}(0)\rangle] + d_0^2\sum_{\mathbf{k}}[\langle T_\tau \tilde{e}^\dagger_{\alpha\bar{\mathbf{k}}}(\tau)\tilde{e}_{\alpha\bar{\mathbf{k}}}(0)\rangle + \langle T_\tau \tilde{d}_{\alpha\mathbf{k}}(\tau)\tilde{d}^\dagger_{\alpha\mathbf{k}}(0)\rangle + \langle T_\tau \tilde{e}^\dagger_{\alpha\bar{\mathbf{k}}}(\tau)\tilde{d}^\dagger_{\alpha\mathbf{k}}(0)\rangle + \langle T_\tau \tilde{d}_{\alpha\mathbf{k}}(\tau)\tilde{e}_{\alpha\bar{\mathbf{k}}}(0)\rangle] = 0.$$

As a result, the Green's function of the $\tilde{p}_\sigma$ boson in $\Lambda^{\rm incoh}_{\alpha\sigma}$ given in Eq. (A4) can be expressed in terms of those of the $\tilde{d}$-$\tilde{e}$ bosons, leading to

$$\Lambda^{\rm fluc}_{\alpha\sigma}(\tau) = \sum_{\mathbf{q}}\{\rho^e_{\alpha\sigma}\langle T_\tau \tilde{e}^\dagger_{\alpha\bar{\mathbf{q}}}(\tau)\tilde{e}_{\alpha\bar{\mathbf{q}}}(0)\rangle + \rho^d_{\alpha\sigma}\langle T_\tau \tilde{d}_{\alpha\mathbf{q}}(\tau)\tilde{d}^\dagger_{\alpha\mathbf{q}}(0)\rangle + \rho^{de}_{\alpha\sigma}[\langle T_\tau \tilde{e}^\dagger_{\alpha\bar{\mathbf{q}}}(\tau)\tilde{d}^\dagger_{\alpha\mathbf{q}}(0)\rangle + \langle T_\tau \tilde{d}_{\alpha\mathbf{q}}(\tau)\tilde{e}_{\alpha\bar{\mathbf{q}}}(0)\rangle]\}, \quad \text{(A7)}$$

where

$$\rho^e_{\alpha\sigma} = p^2_{\alpha 0\sigma} - \bar{p}_0^2, \quad \rho^d_{\alpha\sigma} = p^2_{\alpha 0\bar{\sigma}} - \bar{p}_0^2,$$
$$\rho^{de}_{\alpha\sigma} = p_{0\uparrow}p_{0\downarrow} - \bar{p}_0^2, \quad \text{with} \quad \bar{p}_0^2 = 2d_0^4/\left(p^2_{0\uparrow}+p^2_{0\downarrow}\right).$$

The normal and anomalous Green's functions of the fluctuating doublons and holons involved in Eq. (A7) can be evaluated using the bosonic QPs defined in Eq. (19). We are thus ready to compute the incoherent ISF in Eq. (A6). Remarkably, at $U = 0$, $p_{0\sigma} = d_0 = e_0 = 1/2$, thus $\rho^e_{\alpha\sigma} = \rho^d_{\alpha\sigma} = \rho^{de}_{\alpha\sigma} = \rho^{ed}_{\alpha\sigma} = 0$ in Eq. (A7) and the incoherent spectral function is therefore completely suppressed, recovering the noninteracting limit.

[1] J. Hubbard, Proc. R. Soc. London A **276**, 238 (1963); **277**, 237 (1964); **281**, 401 (1964); **285**, 542 (1965); **296**, 82 (1967).
[2] W. Brinkman and T. M. Rice, Phys. Rev. B **2**, 4302 (1970).
[3] J. M. Luttinger, Phys. Rev. **121**, 942 (1961).
[4] M. C. Gutzwiller, Phys. Rev. Lett. **10**, 159 (1963).
[5] G. Kotliar, S. Y. Savrasov, K. Haule, V. S. Oudovenko, O. Parcollet, and C. A. Marianetti, Rev. Mod. Phys. **78**, 865 (2006); A. Georges, G. Kotliar, W. Krauth, and M. J. Rozenberg, *ibid.* **68**, 13 (1996).
[6] Z. Y. Meng, T. C. Lang, S. Wessel, F. F. Assaad, and A. Muramatsu, Nature **464**, 847 (2010).
[7] W. Wu, Y.-H. Chen, H.-S. Tao, N.-H. Tong, and W.-M. Liu, Phys. Rev. B **82**, 245102 (2010).
[8] A. Liebsch, Phys. Rev. B **83**, 035113 (2011).
[9] R.-Q. He and Z.-Y. Lu, Phys. Rev. B **86**, 045105 (2012).
[10] S.-L. Yu, X.-C. Xie, and J.-X. Li, Phys. Rev. Lett. **107**, 010401 (2011).
[11] W. Wu, S. Rachel, W. M. Liu, and K. Le Hur, Phys. Rev. B **85**, 205102 (2012).
[12] S. Sorella, Y. Otsuka, and S. Yunoki, Sci. Rep. **2**, 992 (2012).
[13] K. Seki and Y. Ohta, J. Korean Phys. Soc. **62**, 2150 (2012).
[14] S. R. Hassan and D. Sénéchal, Phys. Rev. Lett. **110**, 096402 (2013).
[15] A. Liebsch and W. Wu, Phys. Rev. B **87**, 205127 (2013); A. Liebsch, Phys. Rev. Lett. **111**, 029701 (2013).
[16] D. Vollhardt, Rev. Mod. Phys. **56**, 99 (1984).
[17] G. Kotliar and A. E. Ruckenstein, Phys. Rev. Lett. **57**, 1362 (1986).
[18] T. A. Kaplan, P. Horsch, and P. Fulde, Phys. Rev. Lett. **49**, 889 (1982).
[19] H. Yokoyama and H. Shiba, J. Phys. Soc. J. **59**, 3669 (1990); H. Yokoyama, M. Ogata, and Y. Tanaka, J. Phys. Soc. Jpn. **75**, 114706 (2006).

[20] M. Capello, F. Becca, M. Fabrizio, S. Sorella, and E. Tosatti, Phys. Rev. Lett. **94**, 026406 (2005).
[21] R. G. Leigh and P. Phillips, Phys. Rev. B **79**, 245120 (2009).
[22] Y. Yamaji and M. Imada, Phys. Rev. B **83**, 214522 (2011).
[23] L. Lilly, A. Muramatsu, and W. Hanke, Phys. Rev. Lett. **65**, 1379 (1990).
[24] We do not use the *different* slave-boson construction proposed originally by Barnes [25,26], since it does not conserve the fermion number and is known to lead to serious unphysical results [27] when charge excitations are present, even for small U [28].
[25] S. E. Barnes, J. Phys. F **6**, 1375 (1976); **7**, 2637 (1977).
[26] Z. Zou and P. W. Anderson, Phys. Rev. B **37**, 627 (1988).
[27] H. Kaga, Phys. Rev. B **46**, 1979 (1992).
[28] A. Vaezi and X.-G. Wen, arXiv:1010.5744; arXiv:1101.1662; J. Wen, M. Kargarian, A. Vaezi, and G. A. Fiete, Phys. Rev. B **84**, 235149 (2011).
[29] M. Lavagna, Phys. Rev. B **41**, 142 (1990).
[30] Because of the properties of the projection operator, the normal ordering of the square roots in the normalization factors is not an issue [17].
[31] R. Frésard and K Doll, in *The Hubbard Model: Its Physics and Mathematical Physics*, edited by D. Baeriswyl *et al.* (Plenum Press, New York, 1995), pp. 385–392.
[32] W. Metzner and D. Vollhardt, Phys. Rev. Lett. **62**, 324 (1989); F. Gebhard, Phys. Rev. B **41**, 9452 (1990).
[33] K. G. Singh and D. S. Rokhsar, Phys. Rev. B **49**, 9013 (1994).
[34] R. Žitko, J. Bonča, and T. Pruschke, Phys. Rev. B **80**, 245112 (2009).
[35] E. Müller-Hartmann, Z. Phys. B **76**, 211 (1989).
[36] H. Park, K. Haule, and G. Kotliar, Phys. Rev. Lett. **101**, 186403 (2008).
[37] J. W. Rasul and T. Li, J. Phys. C **21**, 5119 (1988).
[38] Z. Wang, Y. Bang, and G. Kotliar, Phys. Rev. Lett. **67**, 2733 (1991); Z. Wang, Int. J. Mod. Phys. B **6**, 603 (1992).
[39] C. Lannert, M. P. A. Fisher, and T. Senthil, Phys. Rev. B **64**, 014518 (2001).
[40] P. Phillips, Rev. Mod. Phys. **82**, 1719 (2010).
[41] F. Ronning, C. Kim, D. L. Feng, D. S. Marshall, A. G. Loeser, L. L. Miller, J. N. Eckstein, I. Bozovic, and Z.-X. Shen, Science **282**, 2067 (1998); F. Ronning, K. M. Shen, N. P. Armitage, A. Damascelli, D. H. Lu, Z.-X. Shen, L. L. Miller, and C. Kim, Phys. Rev. B **71**, 094518 (2005).
[42] H. Kuwamoto, J. M. Honig, and J. Appel, Phys. Rev. B **22**, 2626 (1980).
[43] D. B. McWhan, J. P. Remeika, T. M. Rice, W. F. Brinkman, J. P. Maita, and A. Menth, Phys. Rev. Lett. **27**, 941 (1971).
[44] D. B. McWhan, A. Menth, J. P. Remeika, W. F. Brinkman, and T. M. Rice, Phys. Rev. B **7**, 1920 (1973).
[45] G. D. Mahan, *Many-Particle Physics*, 2nd ed. (Plenum Press, New York, 1990).